HAL open science

Efficient extraction of resonant states in systems with defects

Ivan Duchemin, Luigi Genovese, Eloïse Letournel, Antoine Levitt, Simon Ruget

To cite this version:

Ivan Duchemin, Luigi Genovese, Eloïse Letournel, Antoine Levitt, Simon Ruget. Efficient extraction of resonant states in systems with defects. 2022. hal-03611185v2

HAL Id: hal-03611185

https://hal.science/hal-03611185v2

Preprint submitted on 16 Sep 2022

HAL is a multi-disciplinary open access archive for the deposit and dissemination of scientific research documents, whether they are published or not. The documents may come from teaching and research institutions in France or abroad, or from public or private research centers.

L'archive ouverte pluridisciplinaire **HAL**, est destinée au dépôt et à la diffusion de documents scientifiques de niveau recherche, publiés ou non, émanant des établissements d'enseignement et de recherche français ou étrangers, des laboratoires publics ou privés.

Efficient extraction of resonant states in systems with defects

Ivan Duchemin[1], Luigi Genovese[1], Eloïse Letournel[2], Antoine Levitt[2], Simon Ruget[1]

September 16, 2022

Abstract

We introduce a new numerical method to compute resonances induced by localized defects in crystals. This method solves an integral equation in the defect region to compute analytic continuations of resolvents. Such an approach enables one to express the resonance in terms of a "resonance source", a function that is strictly localized within the defect region. The kernel of the integral equation, to be applied on such a source term, is the Green function of the perfect crystal, which we show can be computed efficiently by a complex deformation of the Brillouin zone, named Brillouin Complex Deformation (BCD), thereby extending to reciprocal space the concept of complex coordinate transformations.

1 Introduction

Hamiltonians of non-homogeneous quantum systems generally have a spectrum consisting of two parts: discrete bound states, and continuous scattering states. The bound states are localized in the region around the scatterer, and can therefore be captured numerically by standard discretization methods in a computational box which is sufficiently large. Scattering states, on the other hand, are delocalized, and their efficient numerical approximation requires discretization techniques which are able to capture long-range oscillations. These differences complicate the description of response phenomena that depend sensitively on continuum states, such as scattering cross sections and resonances. In this paper, we will consider methodologies to compute such properties in one-body Hamiltonians of independent particles; nonetheless, the motivation and the expected applications come from mean-field models such as time-dependent density functional theory (TDDFT).

As a concrete example, consider a one-body (possibly mean-field) Hamiltonian $\hat{H}$, describing for instance a molecule or a defect in a solid. Many time-dependent response properties can be described by sums of functions of the type

$$f(E) = \lim_{\eta \to 0^+} \langle \psi_0 | (E + i\eta - \hat{H})^{-1} | \psi_0 \rangle \tag{1}$$

where ψ_0 can be expressed via a localized function. These functions probe the continuous spectrum at energy E: mathematically, we have $\mathrm{Im}(f(E)) = -\pi \langle \psi_0 | d\hat{\mu}_H(E) | \psi_0 \rangle$, where $d\hat{\mu}_H$ is the projection-valued spectral measure associated to $\hat{H}$. When the Hamiltonian can be interpreted as a small perturbation of a reference Hamiltonian that has both bound and continuous states at the same energy E (for instance, a Hamiltonian where a molecule is surrounded by infinitely high potential barriers, or where a crystalline defect is disconnected from the host crystal), the coupling between these states typically results in a bump of f near E. This corresponds to a resonance, which can be formally defined as a pole in the analytic continuation of f from the upper complex plane into the lower [1].

Resonant states can be found in many areas of Quantum Physics. Also referred to as "Gamow vectors" or "Siegert states", they can be defined for isolated systems as solutions of the time-independent Schrödinger equation subject to outgoing boundary conditions. Described at first by Gamow [2] via quasi-stationary

[1]Univ. Grenoble Alpes, CEA, IRIG-MEM-L Sim, 38054 Grenoble, France
[2]Inria Paris and Université Paris-Est, CERMICS, Ecole des Ponts ParisTech, Marne-la-Vallée, France

states, the concept of resonant states has been widely developed in the field of atomic and nuclear physics (see e.g. Ref. [3]), then adopted for the analysis of scattering properties of quantum systems with open boundaries [4]. Various literature has shown that Siegert states *encode* in compact form the response properties of a system [5, 6]. In particular, the analytic structure of the resolvent operator (i.e. the Green's function) is completely determined by resonant energies and wavefunctions. In the words of Ref. [7], resonant states expansions offer the "possibility of a unified description of bound states, resonances, and continuum spectrum in terms of a purely discrete set of states". For one-body Hamiltonians of quantum systems, the identification of resonant energies and wavepackets would unlock efficient computational aproaches for perturbation theory which would preserve the physico-chemical meaning of the configuration interaction space.

From the perspective of the extraction of physical observables that can be compared to experiments, the computation of functions of the form (1), and a fortiori of their analytic continuation to the lower E complex plane, is challenging. This is because the truncation of $\hat{H}$ to a finite region of space will discretize the energy spectrum, in which case the definition of f above is very singular. This is related to qualitative differences in wave propagation described by the full and truncated Hamiltonians. In unbounded domains, waves propagate to infinity at large times; this results in the correlations $\langle\psi_0|e^{-i\hat{H}t}|\psi_0\rangle$ decaying to zero in time, and therefore f is a smooth function of energy. In bounded domains however, standing waves form at discrete energies and correlation functions do not decay in time.

Practical computations can be performed by approximating $f(E)$ by $f(E+i\eta)$ for some finite $\eta > 0$, which acts as an artificial dissipation parameter, homogeneous to an inverse time. This makes possible the computation of $f(E+i\eta)$ by choosing a computational domain whose size must be large compared to the mean free path of the waves (proportional to $1/\eta$ times the group velocity of the waves). The resulting scheme requires a delicate balance between η and the size of this computational domain. Furthermore, all analytic information in the lower-half complex plane is lost in this procedure, and the computation of resonances requires a potentially numerically unstable extrapolation from the upper complex plane to the lower.

More sophisticated numerical schemes have been developed, sometimes with different names depending on their communities of origin. A first variation of the dissipation method, known as complex absorbing potential [8], is to replace $\hat{H}$ by $\hat{H}+\eta\hat{V}_{\mathrm{CAP}}(x)$, where $\hat{V}_{\mathrm{CAP}}(x)$ is non-zero only outside of a central region. This has similar properties to the above-mentioned technique of a uniform η, but does not modify the operator in the defect region, and can therefore be preferable in practice.

A second technique is to exploit the analytic continuation of the solution to complex numbers to transform scattering or resonant states into localized states [9]. This is done by replacing the space variable x by $xe^{i\theta}$. In this complex scaling approach, the continuous spectrum of the non self-adjoint operator $\hat{H}_\theta$ is moved from $\mathbb{R}^+$ to $e^{-2i\theta}\mathbb{R}^+$, allowing for the computation of functions f as above as well as direct computation of resonances. This can either be done on the whole space, or only on the exterior of a central region; the resulting scheme is then called exterior complex scaling, or perfectly matched layers.

Finally, a third class of methods is to eliminate the degrees of freedom outside of a computational domain. At the discrete level, this is done by a Schur complement approach, while at the continuous level this corresponds to Dirichlet-to-Neumann (DTN) maps [10]. This is especially attractive in simple geometries (such as one-dimensional or three-dimensional in radial coordinates), where the DTN corresponds to a simple local mixed boundary condition.

None of these schemes are fully satisfactory, in particular for the study of defects in quantum systems. The "black-box" approach of adding an artificial dissipation requires a complicated convergence study with respect to the dissipation parameter η (the so-called η trajectories) and may necessitate very large computational domains to obtain stable results. Both the complex scaling as well as the DTN approaches require a particular form for the operator outside of the computational domain, with the DTN method even requiring the analytic solution of the equation. This is particularly problematic in the case where $\hat{H}$ is not fully homogeneous in space outside of a central region, but only periodic, as is the case for defects in solids. Since the exterior problem can be solved in something resembling a closed form only on half-spaces, one has to resort to a matching procedure that makes it impossible to compute resonances directly [11] in dimensions greater than one. In particular, the computation of the DTN map for a periodic operator on the outside of an arbitrary

rectangular domain seems to be a computationally intractable problem.

In this paper, we introduce an integral equation formalism which bypasses such difficulties by an *algebraic* rather than *geometric* splitting: instead of considering the interior and the exterior problem separately, we rather split the Schrödinger operator as $\hat{H} = \hat{H}_0 + \hat{V}$, where $\hat{V}$ is localized only in the central region. This reformulates the problem as an integral equation posed in the central region, similar to the Lippman-Schwinger method used in scattering problems.

The kernel of this integral equation is given by the Green function $R_0(\cdot, \cdot; z)$ of the Hamiltonian $\hat{H}_0$ of the periodic crystal, possibly extended the lower complex plane of energies z. The Green function can be expressed as an integral over the Brillouin zone, which we deform using a multi-dimensional generalization of the Cauchy integral formula. To our knowledge, this is the first numerical method able to do so in the multidimensional case. We choose the deformation function $\mathbf{k} \mapsto \mathbf{k} + i\mathbf{h}(\mathbf{k})$ so that the singularities of R_0 get pushed down into the lower complex plane for z, extending the domain of validity of the integral formula to the continuation of R_0. These complex variable techniques have long been used in theoretical studies [12, 13, 14]. A similar approach has recently been used as a numerical method in 1D scattering problems [15]. We demonstrate in the Appendix A that it can be interpreted as a natural generalization of the complex scaling method to non-parabolic dispersion relations. The resulting scheme only requires unit cell computations, and proves very efficient in practice.

The outline of the paper is as follows. First, we introduce the reformulation to an integral equation in a general setting in Section 2. Then we apply it to the model case of a local perturbation of the free Laplacian, and compare it to an established method (complex scaling) in Section 3. We introduce the Brillouin zone Complex Deformation (BCD) algorithm in Section 4, and apply it to example problems (one-dimensional chain and two-dimensional graphene) in Section 5. In the Appendix A, we reinterpret the BCD method as a generalization of the complex scaling method.

2 Method

2.1 Statement of the problem

We consider the abstract setting of a Hamiltonian

$$\hat{H} = \hat{H}_0 + \hat{V}$$

where the underlying Hilbert space can be discrete or continuous. We assume that $\hat{H}_0$ has a (continuous or discrete) translation invariance (which makes the wavenumber a good quantum number for the eigenstates of $\hat{H}_0$), and that $\hat{V}$ is localized in a region of space. In particular, we will consider three typical cases:

1. Molecular hamiltonians, where $\hat{H}_0 = \hat{T}$ represents the kinetic operator, and is self-adjoint on $L^2(\mathbb{R}^d)$, and $\hat{V}$ is a (local or nonlocal) potential modeling the Coulomb attraction by nuclei, plus possibly Hartree or exchange-correlation terms at the mean-field level.

2. Crystal hamiltonians, where $\hat{H}_0 = \hat{T} + \hat{V}_{\text{per}} + V$ where $\hat{V}_{\text{per}}$ is periodic in space, representing the background potential created by a perfect crystal, and $\hat{V}$ is the potential created by a crystallographic point defect.

3. Tight-binding models, which can be thought of as simplifications of the above crystalline model (e.g. through expansion of the orbitals in a basis of Wannier functions). Here the state space is discrete, with M degrees of freedom at each point of a discrete lattice: the underlying Hilbert space is isomorphic to $\ell^2(\mathbb{Z}^d, \mathbb{C}^M)$. $\hat{H}_0$ is periodic in the sense that for each $\mathbf{R}, \mathbf{R}' \in \mathbb{Z}^d$, the $M \times M$ matrix $H_0(\mathbf{R}, \mathbf{R}')$ satisfies the property $H_0(\mathbf{R}, \mathbf{R}') = H_0(\mathbf{R} + \mathbf{T}, \mathbf{R}' + \mathbf{T})$ for all $\mathbf{T} \in \mathbb{Z}^d$. Here also the (local or nonlocal) potential models a point defect.

By suitable modifications of the definitions of $\hat{H}_0$ and $\hat{V}$, the above setup can be easily modified to accomodate cases that do not fit exactly (see for instance Section 5.2 for the example of an adatom in graphene). We assume that $\hat{H}$ is real (although the extension to complex Hamiltonians poses no difficulty).

Since $\hat{H}$ is self-adjoint, its resolvent

$$\hat{R}(z) = (z - \hat{H})^{-1}$$

is well-defined as a bounded operator when $\mathrm{Im}(z) > 0$. Its kernel $R(\mathbf{r}, \mathbf{r}'; z)$ is localized, in the sense that $R(\mathbf{r}, \mathbf{r}', z) \to 0$ when $|\mathbf{r} - \mathbf{r}'| \to \infty$. This well-known fact is referred to as Combes-Thomas estimates in the mathematical physics literature [16]. In fact, this decay is exponential, with a decay rate related to the imaginary part of z.

As z approaches the spectrum of $\hat{H}$, the resolvent diverges; in fact,

$$\|\hat{R}(z)\| = \sup_{\||\psi\rangle\|=1} \|\hat{R}(z)\,|\psi\rangle\,\| = \frac{1}{\mathrm{dist}(z, \sigma(\hat{H}))}$$

where $\sigma(\hat{H})$ is the spectrum of $\hat{H}$ [17]. This is linked to delocalization of the kernel of $\hat{R}(z)$. However, the kernel of $\hat{R}(z)$ can sometimes be continued analytically beyond the real axis [1, 12]; it is then typically exponentially growing. Accordingly, if $|\psi\rangle$ is an arbitrary localized test vector, then the function

$$\langle\psi|\,\hat{R}(z)\,|\psi\rangle\,,$$

defined as a holomorphic function on the upper complex plane, can sometimes be extended analytically through the essential spectrum into the lower complex plane. This analytic continuation can have poles, which are typically insensitive to the choice of $|\psi\rangle$. We call such a pole z_0 a resonance energy, and the projector on the resonant states can be identified from the residue of $\hat{R}$ around z_0. The resonant states are delocalized solutions of the Schrödinger equation with a complex energy; the imaginary part of z_0 is inversely proportional to their lifetime.

2.2 Computation of resonances

To compute resonances, we first use the following identity among operators:

$$\hat{R}(z) = \hat{R}_0(z)(\hat{1} - \hat{V}\hat{R}_0(z))^{-1} \tag{2}$$

for z in $\mathbb{C}^+$, where $\hat{R}(z) = (z - \hat{H})^{-1}$ and $\hat{R}_0(z) = (z - \hat{H}_0)^{-1}$. This identity is variously known as a resolvent identity, the Dyson equation, or the Duhamel formula, and can be seen as an operator version of the Lippmann-Schwinger equation. If $\hat{R}_0(z)$ can be extended analytically to the lower complex plane of z, then resonances can be found by solving the equation

$$\boxed{|\varphi(z)\rangle = \hat{V}\hat{R}_0(z)\,|\varphi(z)\rangle} \tag{3}$$

for z and $|\varphi(z)\rangle$. The main interest of this formulation is that, by construction, the "resonance source" term $|\varphi(z)\rangle$ is localized in the defect region where the support of $\hat{V}$ lies, which is not the case of the resonant vector $|\psi(z)\rangle = \hat{R}_0(z)\,|\varphi(z)\rangle$, a delocalized eigenvector of $\hat{H} = \hat{H}_0 + \hat{V}$ (the resonant state).

Consider now a simple resonance at z_0 (such that the dimension of the kernel of $\hat{1} - \hat{V}\hat{R}_0(z_0)$ is 1). As $|\varphi(z_0)\rangle$ is not directly associated to a physical state, its normalization is not well defined. However, it is useful to normalize it such that the resolvent has the asymptotic form

$$\hat{R}(z) \approx \frac{1}{z - z_0}|\psi(z_0)\rangle\langle\overline{\psi(z_0)}| \tag{4}$$

close to z_0.

From calculations detailed in Appendix B, this holds as long as

$$\langle\overline{\psi(z_0)}|\hat{V}\hat{R}_0'(z_0)|\varphi(z_0)\rangle = -1 \tag{5}$$

This condition fixes the magnitude and phase of $|\varphi\rangle$ and $|\psi\rangle$ up to sign.

To find resonances, we need to (a) discretize $|\varphi\rangle$; (b) compute the action of the analytic continuation of $\hat{R}_0(z)$; and (c) solve the equation (3). The first task (a) is standard since $|\varphi\rangle$ is localized, and can be done using any method used to compute ground-state properties. Task (c) takes the form of a nonlinear eigenvalue problem $A(z)x = 0$. For small systems, one can simply solve for $\det(A(z)) = 0$. For larger systems where determinants might be ill-conditioned or hard to compute, one can use nonlinear eigensolvers (for instance, applying Newton's method to the set of equations $A(z)x = 0, \|x\| = 1$). Solving nonlinear eigenproblems is a well-studied topic with a variety of efficient algorithms [18]. The task we will focus on is therefore (b), the computation of the analytic continuation of $\hat{R}_0(z)$.

3 Free Laplacian

3.1 Theory

Before tackling periodic problems, we consider a simple one-dimensional model where $\hat{R}_0$ is explicit. We emphasize that this case can be treated using other methods than the one presented here (see for instance [9]), and is simply presented as a test bed for understanding the methodology. The Hamiltonian is the following:

$$\hat{H} = \hat{T} + \hat{V},$$

and we assume that $\hat{V}$ is a localized potential.

Let us first study the situation where the unperturbed Hamiltonian is $\hat{H}_0 = -\Delta$, with resolvent kernel R_0. For $\mathrm{Im}(z) > 0$, consider the equation

$$(z + \Delta)S(\mathbf{r}) = \delta_0(\mathbf{r})$$

Together with the boundary condition that S must go to zero at infinity, this equation admits a single solution for z in the upper complex plane:

$$S_1(\mathbf{r}) = \frac{e^{i\sqrt{z}|\mathbf{r}|}}{2i\sqrt{z}},$$

where we choose the convention $\arg(\sqrt{z}) \in (-\frac{\pi}{2}, \frac{\pi}{2})$. For z in the lower complex plane, the only localized solution would be

$$S_2(\mathbf{r}) = -\frac{e^{-i\sqrt{z}|\mathbf{r}|}}{2i\sqrt{z}}$$

Note that the definition of the Green function differs between the upper and lower complex planes. When z is continued from the upper to the lower complex plane through the negative real axis, S_1 and S_2 match; however, when the continuation is performed through the positive real axis (the spectrum of $\hat{H}_0$), they differ. This gives S the structure of a multivalued function, a Riemann surface of the same type as the square root function, with a singularity at 0.

From the above considerations, for $\mathrm{Im}(z) > 0$ we have

$$R_0(\mathbf{r}, \mathbf{r}'; z) = \frac{e^{i\sqrt{z}|\mathbf{r}-\mathbf{r}'|}}{2i\sqrt{z}}$$

with an artificial branchcut on $\mathbb{R}^-$ and a singularity (branchpoint) at 0. This formula can be continued across the positive real axis (where the kernel explodes as a function of $|\mathbf{r} - \mathbf{r}'|$). When $\hat{V}$ is compactly supported, using the identity (2) together with the analytic Fredholm theory, one can show (Theorem 2.2 of [1]) that R extends to a meromorphic function (holomorphic except for a countable set of points at which

R has finite-order poles, the resonances) across the real axis. Using the method in Section 2.2, the equation (3) for $|\varphi\rangle$ becomes a Fredholm integral equation

$$\varphi(\mathbf{r}) = \frac{1}{2i\sqrt{z}} V(\mathbf{r}) \int_{\mathbb{R}} e^{i\sqrt{z}|\mathbf{r}-\mathbf{r}'|} \varphi(\mathbf{r}') d\mathbf{r}' \tag{6}$$

for z in the lower complex plane. As a shorthand we have omitted the explicit dependence of φ on z.

3.2 Application

We illustrate on the example of a double-well potential $V(x) = 2(e^{-(\frac{x}{2})^2} - e^{-x^2})$ as shown in Figure 1, for which we expect resonances localized in the middle of the well.

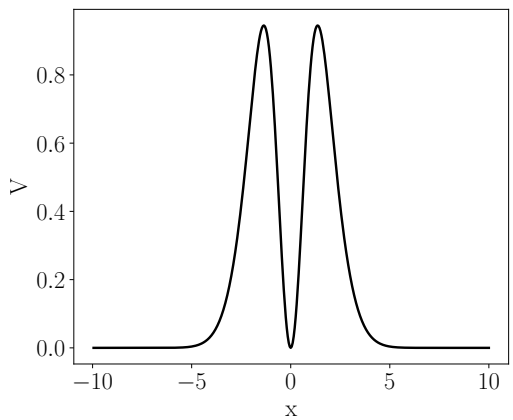

Figure 1: Potential $V(x)$.

To acknowledge the capability of our method to capture physically relevant states, we compare our results to the uniform complex scaling method, which rotates the Hamiltonian in the complex plane and looks for eigenvalues of the non-hermitian operator,

$$\hat{H}_\theta = \hat{S}_\theta \hat{H} \hat{S}_\theta^{-1} = -e^{2i\theta}\Delta + V(xe^{i\theta})$$

The complex scaling operator $\hat{S}_\theta$ is given by the real space representation

$$(S_\theta f)(x) = f(xe^{i\theta})$$

This transformation leaves the discrete spectrum and the resonances of $\hat{H}$ invariant, but rotates the continuous spectrum of $\hat{H}$ by an angle -2θ. Eigenvalues in the lower complex plane which used to be on the lower Riemann surface of the Green function can thus appear as eigenvalues of the rotated Hamiltonian. For our comparison we discretize $\hat{H}_\theta$ using simple finite differences with step h in a domain $[-\frac{L}{2}, \frac{L}{2}]$, and use $\theta = \pi/5$ throughout. For our method, we solve the integral equation (6) using finite differences on the same grid.

We display our results Figure 2. For our method, we plot the smallest singular value of the discretization of $\hat{1} - \hat{V}\hat{R}_0(z)$, which is zero at resonances. In Figure 2, two types of poles and eigenvalues can be seen. For the two closest to the real axis, both methods give the same location, and this location is stable as the box size L is increased. Lower poles are spurious. Those given by our method narrow and plummet more steeply when L goes to infinity. With complex scaling, the angle of the line is stable with L, but the poles tighten up as well. The well-known complex virial theorem [9] can be employed to distinguish spurious poles from actual resonances without recurring to multiple calculations with varying L.

We focus on the two most shallow resonances , denoted by $p_1 \approx 0.68 - 0.13i$ and $p_2 \approx 1.45 - 1.21i$ in Figure 2. We display in Figure 3 the function φ associated to the resonant source term of the eigenvector

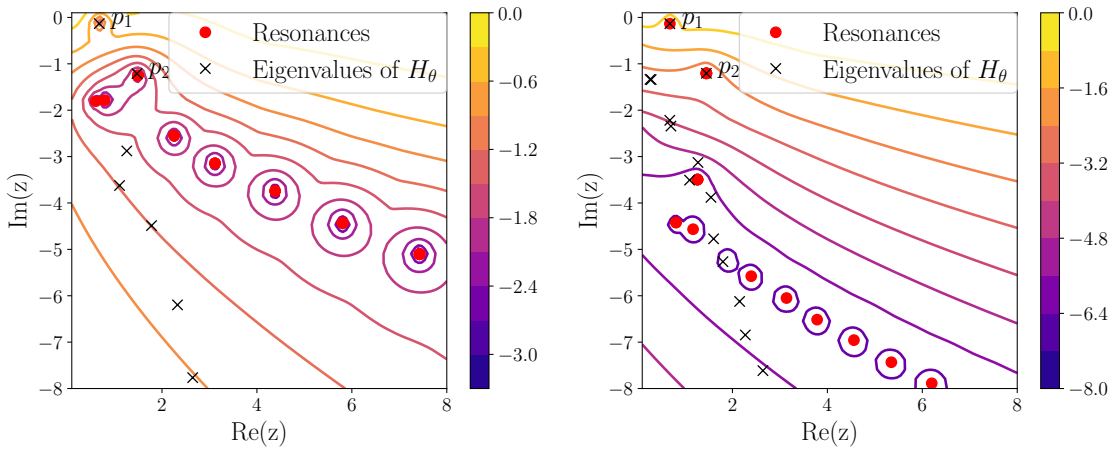

(a) Resonances for $L = 10$, $h = 0.05$

(b) Resonances for $L = 20$, $h = 0.05$.

Figure 2: Base 10 logarithm of the smallest singular value of $1 - \hat{V}\hat{R}_0(z)$, and eigenvalues of the complex scaled $\hat{H}_\theta$ with $\theta = \pi/5$. Resonances as well as spurious poles are visible for both methods. The spurious poles do not converge with L, whereas the resonances do.

with eigenvalue 0 for the operator $\hat{1} - \hat{V}\hat{R}_0$ at the pole, as well as the resonant function ψ. φ is localized on the support of V, and ψ diverges (slowly since $\mathrm{Im}(z) = 0.13$) at infinity. We also show the eigenvector ψ_θ of the rotated Hamiltonian (obtained with complex scaling) associated to the resonance.

To estimate the computational feasibility of our approach, we have also compared in Figure 3 the convergence rate of the resonant energy p_1 as a function of the box size. The grid size h is kept fixed. At finite h, both methods converge to a slightly different value of the resonance energy, and convergence is assessed relative to the fixed-h value. The asymptotic convergence profile is related to the decay of the respective objects discretized: Gaussian-like for the Green function method, which discretizes $\phi = V\psi$, and exponential for the complex scaling method, which discretizes ψ_θ. This gives a better asymptotic convergence for our method than for the complex scaling. The performances of our method in small simulation boxes are equivalent or slightly below those obtained by complex scaling. We however caution here that our aim is not a direct comparison of the performances of the two methods, which is a case-study-dependent investigation that goes beyond the scope of our paper. It is enough for our purposes to show that the computational complexity of our method is comparable to that of other equivalent approaches.

To summarize, such an approach enables us to *directly* access to the resonant wavefunction and energies, without the need to transform the Hamiltonian in complex space, and by working on a computational domain which coincides with the support of the potential. In order to do that, we need to express R_0 (otherwise stated the Green function of the Helmholtz Equation) for z in the lower half of the complex plane in the desired region, and filter the spurious poles with usual techniques, like the complex virial theorem.

4 Periodic media

We now consider the case where

$$\hat{H} = \hat{H}_0 + \hat{V}$$

with $\hat{H}_0$ a periodic operator and $\hat{V}$ a localized potential. Although our method applies to continuous models of the form $-\Delta + V_{\mathrm{per}}(\mathbf{r}) + V(\mathbf{r})$, with V_{per} being a function having the periodicity of a lattice, we will present the method using a discrete tight-binding model (discrete Schrödinger operator) where Γ is a d-dimensional lattice. This is done to minimize numerical issues related to the discretization of the unit cell, and to

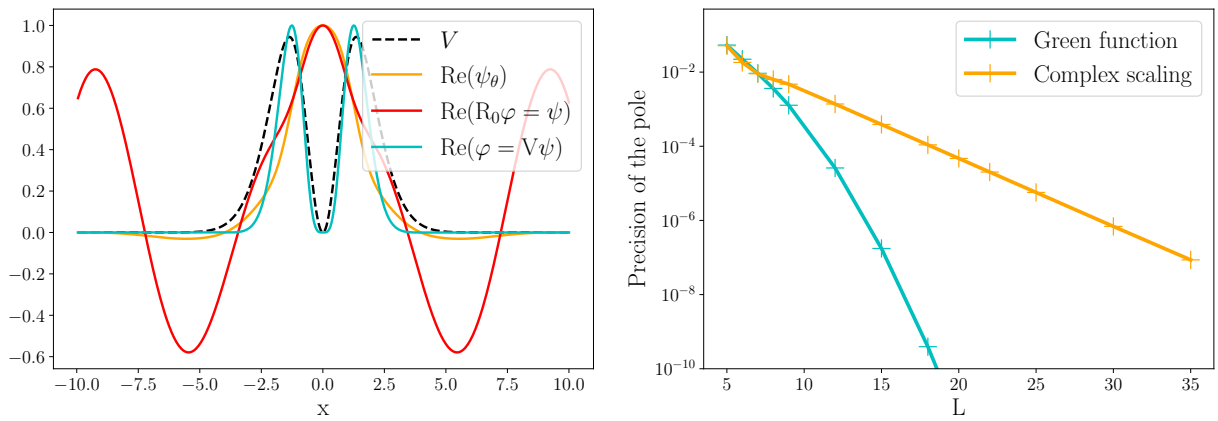

(a) Results for p_1.

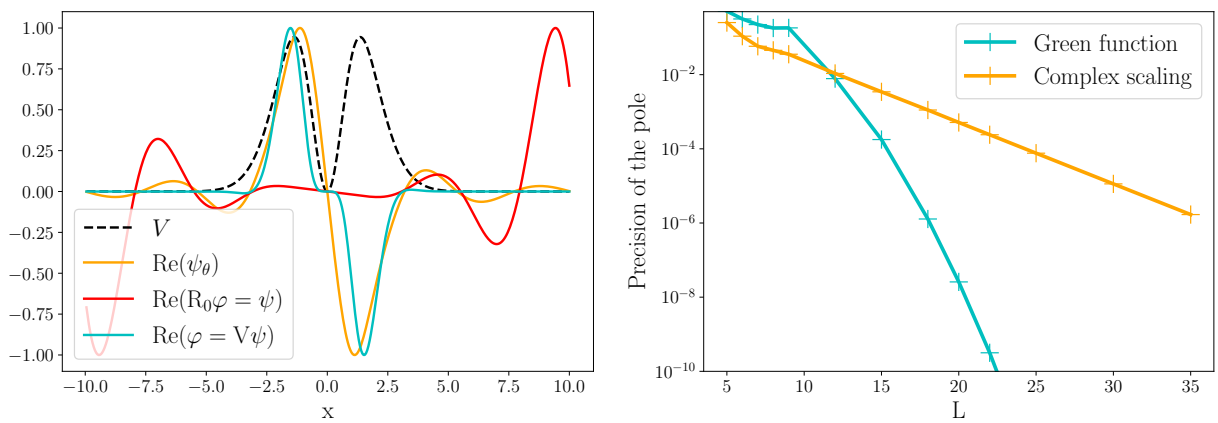

(b) Results for p_2.

Figure 3: Resonant states and convergence rates for the two first poles p_1 and p_2, for the two methods ($h = 0.05$). Left panel: potential (black dashed line), resonant state ψ (red), $\varphi = V\psi$ (blue) and rotated resonant state ψ_θ (yellow). Right panel: convergence of the pole location as a function of the box size. The normalization of the states is arbitrary and done for plotting clarity.

simplify the exposition. We refer to the conclusion for perspectives in applying our method to continuous Hamiltonians.

The tight-binding models we consider have M internal degrees of freedom per lattice site $\mathbf{R} \in \Gamma$, with a lattice Γ isomorphic to $\mathbb{Z}^d$. The Hilbert space is $\ell^2(\Gamma, \mathbb{C}^M)$ with wavefunctions indexed by the lattice site $\mathbf{R} \in \Gamma$ and the degree of freedom $i \in \{1, \ldots, M\}$. For each $\mathbf{R}, \mathbf{R}' \in \Gamma$, $H_0(\mathbf{R}, \mathbf{R}')$ is a $M \times M$ matrix satisfying

$$H_0(\mathbf{R}, \mathbf{R}') = H_0(\mathbf{R} + \mathbf{T}, \mathbf{R}' + \mathbf{T})$$

for all $\mathbf{T} \in \Gamma$.

4.1 Green function of a periodic Hamiltonian

Since $\hat{H}_0$ is periodic, we can label its states as Bloch waves $\psi_{n\mathbf{k}}(\mathbf{R}) = e^{i\mathbf{k}\cdot\mathbf{R}} u_{n\mathbf{k}}(\mathbf{R})$ where $u_{n\mathbf{k}} \in \mathbb{C}^M$ is normalized [19]. The index $\mathbf{k}$ enumerates the Brillouin zone $\mathcal{B}$, a unit cell of the reciprocal lattice Γ^* (the set of $\mathbf{K} \in \mathbb{R}^d$ such that $\mathbf{K}\cdot\mathbf{T}$ is a multiple of 2π for all $\mathbf{T} \in \Gamma$). The $u_{n\mathbf{k}}$ are the orthonormal solutions of

$$H_{0,\mathbf{k}} \left|u_{n\mathbf{k}}\right\rangle = \varepsilon_{n\mathbf{k}} \left|u_{n\mathbf{k}}\right\rangle \tag{7}$$

where the reciprocal-space kernel $H_{0,\mathbf{k}} \in \mathbb{C}^{M\times M}$ is the Fourier transform of $H_0(\mathbf{0},\cdot)$:

$$H_{0,\mathbf{k}} = \sum_{\mathbf{T}\in\Gamma} e^{i\mathbf{k}\cdot\mathbf{T}} H_0(\mathbf{0},\mathbf{T}). \tag{8}$$

Conversely, we have

$$H_0(\mathbf{R},\mathbf{R}') = \frac{1}{|\mathcal{B}|}\int_{\mathcal{B}} e^{i\mathbf{k}\cdot(\mathbf{R}-\mathbf{R}')} H_{0,\mathbf{k}} d\mathbf{k}$$

and therefore, when $\mathrm{Im}(z) > 0$,

$$R_0(\mathbf{R},\mathbf{R}';z) = \frac{1}{|\mathcal{B}|}\int_{\mathcal{B}} e^{i\mathbf{k}\cdot(\mathbf{R}-\mathbf{R}')} \frac{1}{z - H_{0,\mathbf{k}}} d\mathbf{k} \tag{9}$$

$$= \frac{1}{|\mathcal{B}|}\int_{\mathcal{B}} e^{i\mathbf{k}\cdot(\mathbf{R}-\mathbf{R}')} \sum_{n=1}^{M} \frac{u_{n\mathbf{k}} u_{n\mathbf{k}}^*}{z - \varepsilon_{n\mathbf{k}}} d\mathbf{k}. \tag{10}$$

When $\mathrm{Im}(z) > 0$, this function can be computed simply by discretizing the integral. This is usually done by a uniform sampling of the Brillouin zone (Monkhorst-Pack grid [20]), a simple quadrature that is very efficient because it integrates explicitly low-order Fourier harmonics and is therefore exponentially accurate for analytic functions [21]. However, as the imaginary part of z decreases to zero, the integrand is more and more singular, with singularities concentrating on the Fermi surface $S(\mathrm{Re}(z))$, where

$$S(E) = \cup_{n=1,\ldots,M} S_n(E) = \left\{\mathbf{k}\in\mathcal{B}, \exists n \in \{1,\ldots,M\}, \varepsilon_{n\mathbf{k}} = E\right\}$$
$$S_n(E) = \left\{\mathbf{k}\in\mathcal{B}, \varepsilon_{n\mathbf{k}} = E\right\}$$

The integration therefore gets less accurate as $\mathrm{Im}(z)$ is reduced. The analytic structure of R_0 is also destroyed by the discretization: the discretized function becomes meromorphic on $\mathbb{C}$, with a finite number of poles at the eigenvalues $\varepsilon_{n\mathbf{k}}$. In particular, the continuation of R_0 for $\mathrm{Im}(z) < 0$ cannot be obtained. Nevertheless, the continuation exists around all energies $E \in \mathbb{R}$ such that the following two conditions hold:

- Bands do not intersect at energy E: $\forall \mathbf{k} \in S(E), \varepsilon_{n\mathbf{k}} = \varepsilon_{m\mathbf{k}} \Rightarrow n = m$;
- The group velocities are nonzero at energy E: $\forall \mathbf{k} \in S(E), \varepsilon_{n\mathbf{k}} = E \Rightarrow \nabla\varepsilon_{n\mathbf{k}} \neq 0$.

Under these conditions, the Fermi surface $S(E)$ is a union of smooth surfaces, and the resolvent can be analytically continued near E [22, 12]. The discrete set of energies E for which one of the conditions above do not hold generally result in branch point singularities, and are called *van Hove singularities*. These conditions make intuitive sense. The resolvent being analytic at a particular energy means that wave propagation at that energy is "regular": Bloch waves have a well-defined non-zero group velocity. The presence of a van Hove singularity can be interpreted as a resonance (anomalous wave propagation) on the real axis. Analytic continuation of the resolvent near these singularity points is not possible [12] or physically meaningful (because the anomalous wave propagation caused by the van Hove singularity effectively hides any possible resonance). Our method is therefore only relevant in the energy regions distant from van Hove singularities.

Taking into account these constraints, we realize the analytic continuation of R_0 in the lower complex plane of z by applying a complex coordinate transformation in the *reciprocal* space

$$\mathbf{k} \to \boldsymbol{\kappa}(\mathbf{k}) = \mathbf{k} + i\mathbf{h}(\mathbf{k}) \ , \tag{11}$$

which does not modify the position of the *singular* points of the transformed dispersion relation $\varepsilon_{n\kappa}$. In other terms, $\boldsymbol{\kappa}(\mathbf{k})$ is defined such as to approach the identity transformation in the vicinity of a van Hove singularity. We call this transformation a Brillouin Complex Deformation (BCD). We now study how to perform the continuation in practice.

4.2 Complex deformation of the Brillouin zone

To remedy the two problems of the naive quadrature (loss of accuracy near the real axis, and loss of analytic continuation), we will deform the integration domain into the complex plane. This is easier to see in one dimension, where the integral (9) can be deformed using the Cauchy formula. Remarkably, this can be extended to higher dimensions:

Lemma 1. *Let $I(\mathbf{k})$ be a Γ^*-periodic function, analytic in an open set $U = \mathbb{R}^d + i[-\eta, \eta]^d$. Then, for all Γ^*-periodic and continuously differentiable functions $\mathbf{h}(\mathbf{k}) : \mathbb{R}^d \to [-\eta, \eta]^d$, we have*

$$\int_{\mathcal{B}} I(\mathbf{k}) d\mathbf{k} = \int_{\mathcal{B}} I(\boldsymbol{\kappa}(\mathbf{k})) \det(\boldsymbol{\kappa}'(\mathbf{k})) d\mathbf{k} = \int_{\mathcal{B}} I(\mathbf{k} + i\mathbf{h}(\mathbf{k})) \det(1 + i\mathbf{h}'(\mathbf{k})) d\mathbf{k}$$

Proof. Consider for $\alpha \in \mathbb{C}$ the function

$$J(\alpha) = \int_{\mathcal{B}} I(\mathbf{k} + \alpha\mathbf{h}(\mathbf{k})) \det(1 + \alpha\mathbf{h}'(\mathbf{k})) d\mathbf{k},$$

analytic for $|\alpha| \leq 1$. For α real, positive and sufficiently small, we have by a change of variables $J(\alpha) = J(0)$. By analytic continuation, it follows that $J(i) = J(0)$. □

Applied to the integrand

$$I_z(\mathbf{k}) = \frac{1}{|\mathcal{B}|} e^{i\mathbf{k}\cdot(\mathbf{R}-\mathbf{R}')} \frac{1}{z - H_{0,\mathbf{k}}},$$

this formula provides an explicit representation of the analytic continuation of $R_0(\mathbf{R}, \mathbf{R}'; z)$ from the upper complex plane to the lower. More explicitly, taking a path $z(t)$ originating from a point in the upper complex plane and descending into the lower plane, the formula

$$R_0(\mathbf{R}, \mathbf{R}'; z) = \frac{1}{|\mathcal{B}|} \int_{\mathcal{B}} I_z(\boldsymbol{\kappa}(\mathbf{k})) \det(\boldsymbol{\kappa}'(\mathbf{k})) d\mathbf{k}$$

provides a continuation of $R_0(\mathbf{R}, \mathbf{R}'; z)$ along the path as long as the eigenvalues of $H_{0,\mathbf{k}+i\mathbf{h}(\mathbf{k})}$ for $\mathbf{k} \in \mathcal{B}$ do not intersect the path. Appropriate choices of $\mathbf{h}$ can therefore extend the region of validity of the integral formula into the lower complex plane. Then, the deformed integral can be discretized in a standard Monkhorst-Pack grid:

$$\begin{aligned} R_0(\mathbf{R}, \mathbf{R}'; z) &\approx \frac{|\mathcal{B}|}{N^d} \sum_{\mathbf{k} \in \mathcal{B}_N} I_z(\boldsymbol{\kappa}(\mathbf{k})) \det(\boldsymbol{\kappa}'(\mathbf{k})) d\mathbf{k} \\ &= \frac{1}{N^d} \sum_{\mathbf{k} \in \mathcal{B}_N} e^{i(\mathbf{k}+i\mathbf{h}(\mathbf{k}))\cdot(\mathbf{R}-\mathbf{R}')} \frac{1}{z - H_{0,(\mathbf{k}+i\mathbf{h}(\mathbf{k}))}} \det(1 + i\mathbf{h}'(\mathbf{k})) d\mathbf{k} \end{aligned}$$

where $\mathcal{B}_N$ is the set of N^d points in the Monkhorst-Pack grid.

The task at hand is now to choose $\mathbf{h}(\mathbf{k})$ so that $\varepsilon_{n,\mathbf{k}+\mathbf{h}(\mathbf{k})}$ avoids all complex numbers z in the path of the analytic continuation we are interested in. As mentioned before, when z approaches the real axis, the integrand concentrates on the Fermi surface. Fix $E \in \mathbb{R}$, and assume that we are interested in the analytic continuation on a line descending from the upper complex plane and passing through E. Assume that $n_0, \mathbf{k}_0$ are such that $\varepsilon_{n_0\mathbf{k}_0} = E$. Then, near $\mathbf{k}_0$, we have

$$\varepsilon_{n_0\mathbf{k}} \approx E + \nabla\varepsilon_{n_0\mathbf{k}_0} \cdot (\mathbf{k} - \mathbf{k}_0)$$

and therefore, for small $\mathbf{h}$ and $\mathbf{k}$ close to $\mathbf{k}_0$:

$$\mathrm{Im}(\varepsilon_{n_0\mathbf{k}+i\mathbf{h}(\mathbf{k})}) \approx \nabla\varepsilon_{n_0\mathbf{k}_0} \cdot \mathbf{h}(\mathbf{k})$$

By choosing $\mathbf{h}(\mathbf{k})$ to be oriented in the direction of $-\nabla\varepsilon_{n_0\mathbf{k}_0}$ in a neighborhood of $\mathbf{k}_0$, we can ensure that $\varepsilon_{n_0\mathbf{k}}$ has a negative imaginary part whenever its real part becomes close to E. When $\varepsilon_{n\mathbf{k}}$ is far from E, we should set $\mathbf{h}(\mathbf{k})$ to zero. We use the general form

$$\mathbf{h}(\mathbf{k}) = -\sum_{n\in 1}^{M} \alpha\nabla\varepsilon_{n\mathbf{k}}\,\chi\left(\frac{\varepsilon_{n\mathbf{k}} - E}{\Delta E}\right) \tag{12}$$

where α and ΔE are constants with $\alpha > 0$, and $\chi(E)$ is a cutoff function, equal to 1 at 0 and zero for large values (in practice, we use a Gaussian).

To summarize, we employ as a definition of our BCD transformation the following function:

$$\boldsymbol{\kappa}(\mathbf{k}; \alpha, E, \Delta E) \equiv \mathbf{k} - i\alpha \sum_{n=1}^{M} \nabla\varepsilon_{n\mathbf{k}}\,\chi\left(\frac{\varepsilon_{n\mathbf{k}} - E}{\Delta E}\right)$$

The appropriate choice of the parameters is not trivial. The parameter α scales the whole deformation. It should ideally be chosen large enough for the deformation to be effective, but choosing it too large invalidates the first-order expansion above. The parameter ΔE must be chosen small enough to restrict the deformation to the surrounding of $\varepsilon_{n\mathbf{k}}$, but choosing it too small results in rapid variations of h and requires a finer discretization of the Brillouin zone to integrate correctly.

For $\mathbf{h}(\mathbf{k})$ to be a smooth function, $\nabla\varepsilon_{n\mathbf{k}}$ should be smooth whenever $\chi(\frac{\varepsilon_{n\mathbf{k}}-E}{\Delta E})$ is nonzero. When ΔE is small, this is possible under the first condition outlined in Section 4.1: near the Fermi surface $S(E)$, bands should not cross, so that $\nabla\varepsilon_{n\mathbf{k}}$ is smooth. In order for the deformation to produce its expected effect, $\nabla\varepsilon_{n\mathbf{k}}$ should not be small at the Fermi level, recovering the second condition in Section 4.1.

More quantitatively, we collect the conditions that α, ΔE and the discretization parameter N should satisfy in order to ensure a good approximation of the analytic continuation of $R_0(\mathbf{R}, \mathbf{R}'; z)$ near an energy E:

- To ensure a smooth $\mathbf{h}$,

$$\Delta E \ll \mathrm{dist}(E, z) \quad \text{for all van Hove singularities } z.$$

- To ensure a valid first-order approximation,

$$\alpha|\nabla\varepsilon_{n\mathbf{k}}| \ll \mathrm{diam}(\mathcal{B}) \quad \forall\mathbf{k} \in S_n(E)$$

- To ensure z remains above the deformed spectrum at first order, when $\mathrm{Im}(z) < 0$,

$$|\mathrm{Im(z)}| \ll \alpha|\nabla\varepsilon_{n\mathbf{k}}|^2 \quad \forall\mathbf{k} \in S_n(E)$$

- To ensure an accurate integration,

$$\frac{\mathrm{diam}(\mathcal{B})}{N} \ll \min\left(\frac{\Delta E}{|\nabla\varepsilon_{n\mathbf{k}}|}, \alpha|\nabla\varepsilon_{n\mathbf{k}}|\right) \quad \forall\mathbf{k} \in S_n(E)$$
$$N \gg |\mathbf{R} - \mathbf{R}'|$$

Even though good results might be obtained even violating these conditions, they give useful rules of thumb to choose the parameters for a given system. Note that at van Hove singularities it is impossible to continue the resolvent. Therefore the procedure outlined above is only applicable outside of singularities, and we will seek resonances there.

5 Applications

We now apply the method developed above to local perturbations of tight-binding Hamiltonians.

5.1 1D tight-binding for a diatomic chain

5.1.1 Perfect crystal

Let us now consider a one dimensional chain containing two types of atoms alternatively. The site energies of the atoms are E_a and E_b, and the electron can hop from one site to another with a hopping constant 1:

$$H_0 = \begin{pmatrix} \ddots & \ddots & \ddots & & & & & \\ & 1 & E_a & 1 & & & & \\ & & 1 & E_b & 1 & & & \\ & & & 1 & E_a & 1 & & \\ & & & & 1 & E_b & 1 & \\ & & & & & \ddots & \ddots & \ddots \end{pmatrix}$$

The Bloch transform of H_0 is

$$H_{0,k} = \begin{pmatrix} E_a & e^{-ik}+1 \\ e^{ik}+1 & E_b \end{pmatrix}$$

with bands

$$\varepsilon_{\pm,k} = \frac{E_a+E_b}{2} \pm \sqrt{\frac{(E_a-E_b)^2}{4} + 4\cos^2\left(\frac{k}{2}\right)}$$

In numerical experiments, we choose $E_a = 1$, $E_b = 0$, so that the continuous spectrum of H_0 is approximately $[-1.56, 0] \cup [1, 2.56]$.

We can apply the method of the previous section to obtain the analytic continuation of the 2×2 matrix $R_0(\mathbf{R}, \mathbf{R}'; z)$. We show in Figure 4 the BCD we use for the energy $E = 2$.

We apply it in Figure 5 to compute the continuation of the trace per unit cell of the Green function

$$\mathrm{Tr}(R_0(0,0;z)) = \frac{1}{|\mathcal{B}|}\int_{\mathcal{B}} \mathrm{Tr}\left(\frac{1}{z - H_{0,\mathbf{k}}}\right) d\mathbf{k}$$

whose imaginary part for real z is equal to $-\pi$ times the density of states. The BCD moves the discretized continuum of poles further down in the complex plane, allowing us to compute the continuation of the resolvent across the spectrum of $\hat{H}_0$.

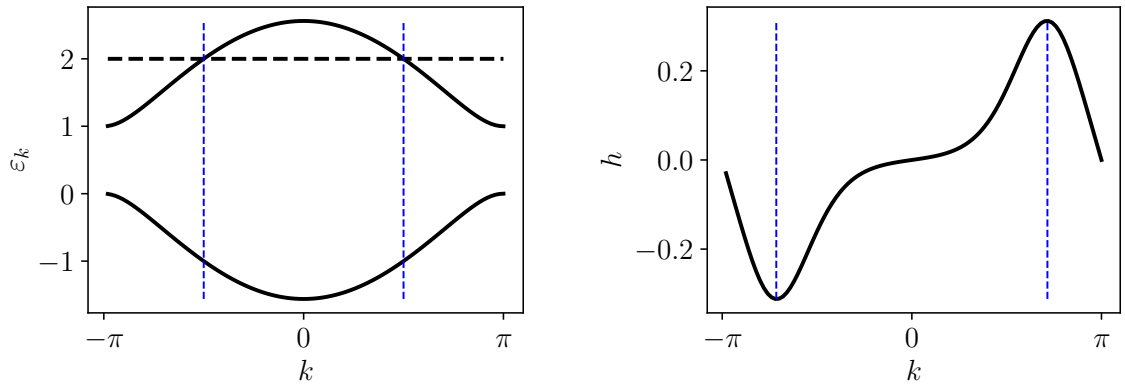

(a) Band structure $\varepsilon_{\mathbf{k}}$.

(b) Profile of $\mathbf{h}$ from (12).

Figure 4: BCD at the energy of interest $E = 2$ for the diatomic chain ($\alpha = 0.4$, $\Delta E = 0.7$, $\alpha = 1$). The contour is deformed in the direction $-\nabla\varepsilon$ near the Fermi surface $S(E)$ (dashed blue lines) at energy E (dashed black line).

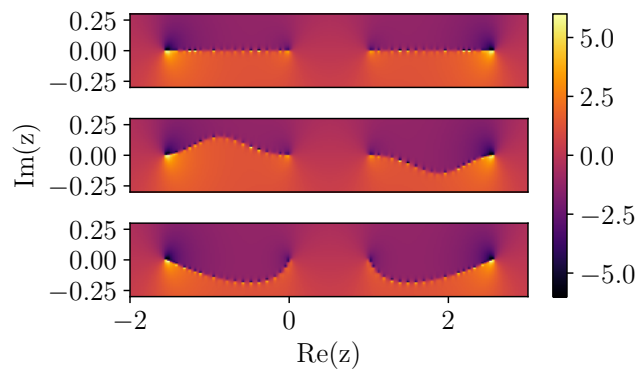

Figure 5: Imaginary part of the trace by cell of the Green function for the diatomic model: with no deformation (top), with a BCD with $E = 2$ (middle), and with $E = \mathrm{Re}(z)$ for every z (bottom). Parameters are $N = 50$, $\alpha = 0.3$, $\Delta E = 0.5$.

5.1.2 Defect

To obtain resonances, we now perturb the system locally in the following manner:

$$H = H_0 + V = \begin{pmatrix} \ddots & & & & & & & & & \\ & \ddots & & & & & & & & \\ \ddots & \ddots & 1 & & & & & & & \\ & 1 & E_a & \epsilon & & & & & & \\ & & \epsilon & E_b & 1 & & & & & \\ & & & 1 & E_a & 1 & & & & \\ & & & & 1 & E_b & 1 & & & \\ & & & & & 1 & E_a & \epsilon & & \\ & & & & & & \epsilon & E_b & 1 & \\ & & & & & & & 1 & \ddots & \ddots \\ & & & & & & & & \ddots & \end{pmatrix} \tag{13}$$

This defect is chosen so that, at $\epsilon = 0$, there is a central region unconnected to the rest of the chain, with four eigenvalues (-1.19, -0.29, 1.29, 2.19), embedded in the continuous spectrum of H_0. At $\epsilon > 0$, the embedded eigenvalues turn into resonances. We show this by plotting the smallest singular value of $\hat{1} - \hat{V}\hat{R}_0(z)$ as a function of z in Figure 6, for $\epsilon = 0.2$. We find resonances close to the eigenvalues at $\varepsilon = 0$, as expected.

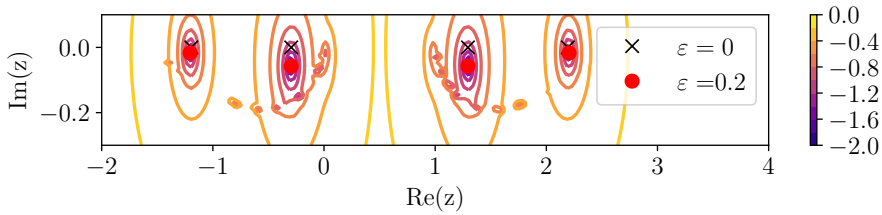

Figure 6: Base 10 logarithm of the smallest singular value of $\hat{1} - \hat{V}\hat{R}_0(z)$, with the same parameters as in Figure 5. The black crosses are eigenvalues at $\varepsilon = 0$, the red dots are resonances at $\varepsilon = 0.2$

For this simple monodimensional model, computing resonances can be done using an explicit computation of the Green function (or of the scattering matrix) through Schur complements. We verified that the results given by our method on a simple case are in agreement with the resonances found with scattering matrices [23].

5.2 Graphene

5.2.1 Perfect crystal

In this section, we study the standard nearest-neighbour model of graphene with hopping parameter t, and lattice vectors $\mathbf{a}_1 = (\sqrt{3}/2, 1/2), \mathbf{a}_2 = (\sqrt{3}/2, -1/2)$. The Bloch transform of the Hamiltonian writes:

$$H_{\mathbf{k}} = \begin{pmatrix} 0 & -t(1 + e^{i\mathbf{k}\cdot\mathbf{a_1}} + e^{i\mathbf{k}\cdot\mathbf{a_2}}) \\ -t(1 + e^{-i\mathbf{k}\cdot\mathbf{a_1}} + e^{-i\mathbf{k}\cdot\mathbf{a_2}}) & 0 \end{pmatrix}$$

The Brillouin zone is a unit cell of the lattice spanned by the reciprocal vectors $\mathbf{b}_1 = 2\pi(1/\sqrt{3}, 1), \mathbf{b}_2 = 2\pi(1/\sqrt{3}, -1)$. In the following, the plots in the Brillouin zone will be given in the reduced coordinate system $\mathbf{k} = k_1\mathbf{b}_1 + k_2\mathbf{b}_2$, in which we take the Brillouin zone as $[-1/2, 1/2]^2$. We take $t = 1$ throughout.

The dispersion relation is represented Figure 7a.

Our BCD, represented in Figure 7b for $E = 2$, allows us to compute the Green function (Figure 8) and therefore the density of states (Figure 9). The density of states (DOS) is defined as

$$D(z) = -\frac{1}{\pi} \lim_{\eta \to 0^+} \mathrm{Im}\left(\underline{\mathrm{Tr}}\left((z + i\eta - H)^{-1}\right)\right)$$

where $\underline{\mathrm{Tr}}$ is the trace by cell of the operator.

The dispersion relation is singular at the two Dirac points, at which the multiplicity of the eigenvalues is double and where the behaviour of the eigenvalues is linear at first order. The BCD method is efficient for the E which are not too close to these singularities or to the other van Hove points, where the gradient vanishes ($E = 0, \pm t, \pm 3t$); the BCD is unable to move these singularities away from the real axis.

We compare the DOS to both the exact analytic formula from [24] and the standard approximation

$$D_{N,\eta}(E) \approx \frac{1}{N^2} \sum_{\mathbf{k} \in \mathcal{B}_N} \sum_{n=1}^{M} g\left(\frac{\varepsilon_{n\mathbf{k}} - E}{\eta}\right)$$

with g a normalized Gaussian and $\mathcal{B}_N$ a Monkhorst-Pack grid with N^2 points. This method converges to the DOS as $N \to \infty$ then $\eta \to 0^+$ (but not the reverse). Optimizing η as a function of N gives a convergence of the DOS as $1/N^2$ outside of the van Hove singularities [25, 22, 26]. By contrast, the BCD method directly gives an exponential convergence as a function of N. Even for small values of N, we observe that the BCD gives more accurate (but less smooth) results.

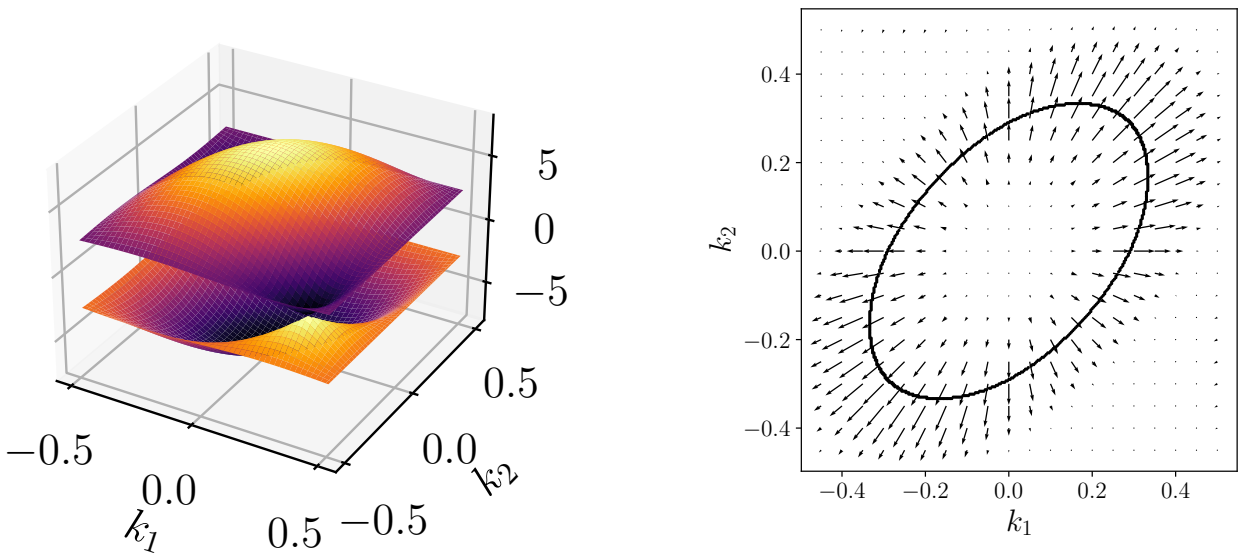

(a) Dispersion relation $\varepsilon(\mathbf{k})$ of graphene.

(b) $\mathbf{h}(\mathbf{k})$ at $E = 2$. The black line is the Fermi surface.

Figure 7: Dispersion relation and BCD for the graphene.

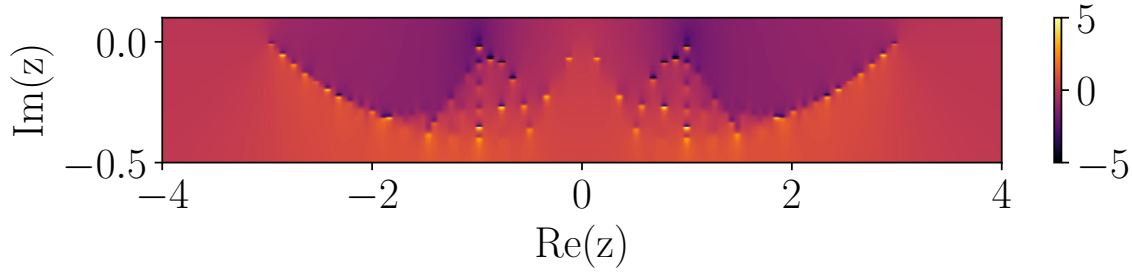

Figure 8: Imaginary part of the trace per unit cell of the Green function for the nearest-neighbor model of graphene. Parameters are $N = 13$, $\alpha = 0.4$, $\Delta E = 0.5$.

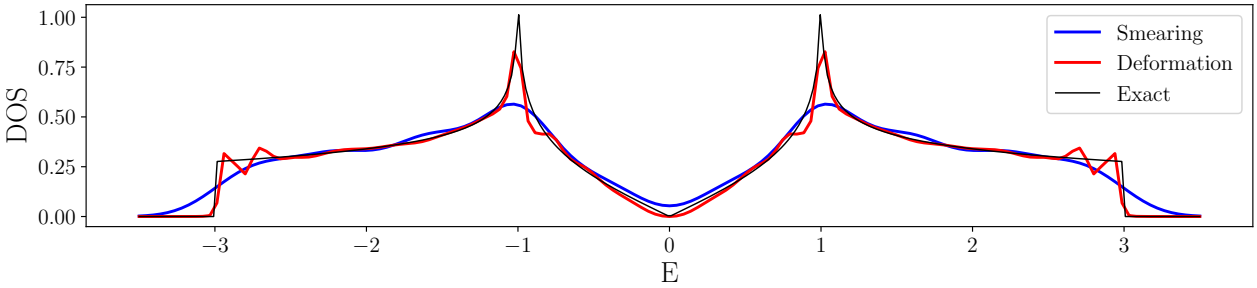

Figure 9: DOS of the nearest-neighbor model of graphene. The red plot is computed with our BCD method ($N = 9$, $\alpha = 0.3$, $\Delta E = 0.4$), and the black plot is the reference DOS. The blue curve is the DOS obtained by the Gaussian smearing method for the same $N = 9$, with an optimized value of $\eta = 0.3$.

5.2.2 Defect

We now put an additional atom (adatom) on the surface of the graphene as a perturbation. We implement this by a new site, linked to a single site of the lattice with a hopping constant ϵ, and a site energy of E_d. This is similar to the "top" configuration of [27]. With a small hopping constant, we expect a resonance, since the configuration $\epsilon = 0$ gives a bound state at energy E_d. We select the defect so that the resonance will be close to $E = 2$ (away from van Hove singularities). Taking $\epsilon = 0.4$, $E_d = 2$, we expect a resonance with a real part close to 2; the Fermi Golden rule can be used to estimate the imaginary part to second order in ε:

$$\mathrm{Im}(z) \approx \varepsilon^2 R_0(0, 0; E_d + i0^+)_{11}.$$

We use the method BCD in the previous section (with the same parameters $\alpha = 0.4, \Delta E = 0.5$) to compute R_0, and obtain approximately $\mathrm{Im}(z) \approx -0.0854i$.

To compute the resonance exactly, we proceed using the same method as before, solving the equation (3). Since the defect $\hat{V}$ only links one site of the lattice to the adatom, we only need to compute one coefficient of the Green function R_0. We look for zeros of $\hat{1} - \hat{V}\hat{R}_0$ in Figure 10, and find a pole near $2.062 - 0.0858i$, which is consistent with the Fermi Golden rule. The convergence of the method (Figure 11) is exponential with respect to N. We plot the resonance state in Figure 12.

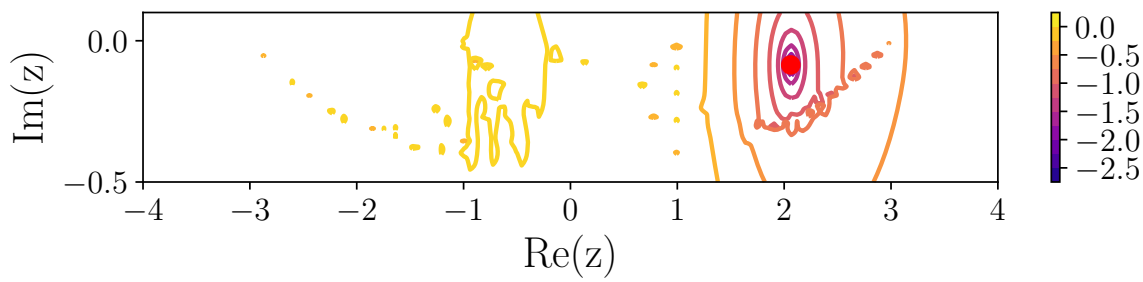

Figure 10: Base 10 logarithm of the smallest singular value of $\hat{1} - \hat{V}\hat{R}_0(z)$ for an adatom on graphene.

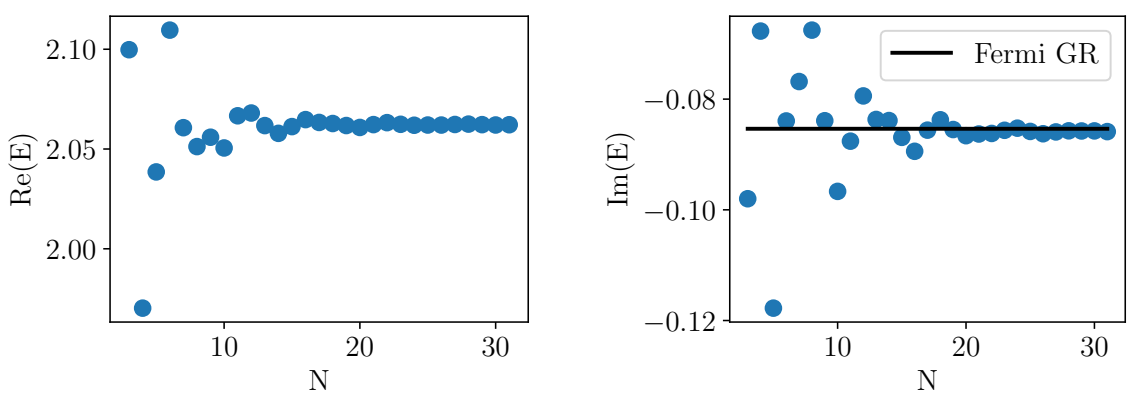

Figure 11: Convergence of the real and imaginary parts of the resonance energy with respect to the discretization parameter of the Brillouin zone N. The prediction of the Fermi Golden rule for the imaginary part of the resonance is given in black on the right panel.

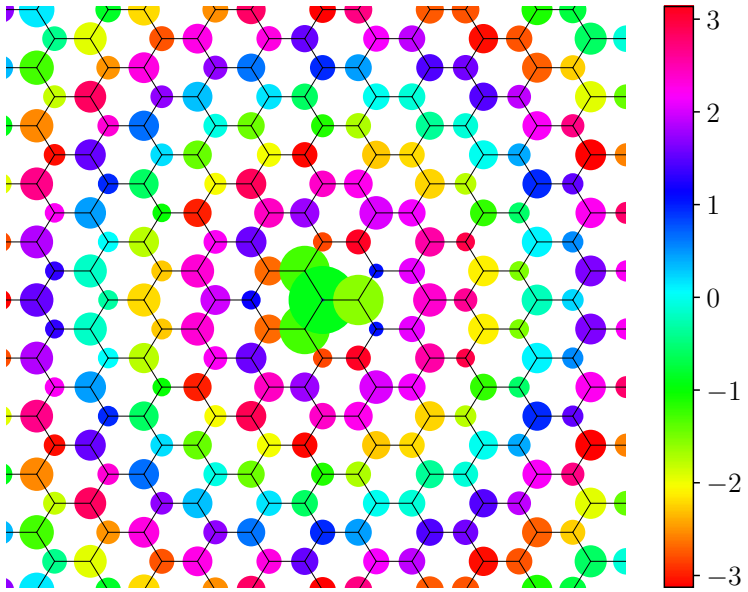

Figure 12: Resonant state. The size of the dots is proportional to the modulus of the state, the color represents the phase.

6 Conclusion

We have introduced a new method to find resonances in solids in the framework of a localized, single defect, and demonstrated its efficiency and generality. The method is based on a reformulation as an integral equation, posed on the support of the defect. The kernel of this integral equation is the Green function of the periodic system, which we compute using a complex deformation of the Brillouin zone. This algebraic (rather than geometric) splitting is very general and applies to every locally perturbed periodic problem. Unlike methods based on introducing artificial dissipation, the BCD-based method is an exact reformulation of the problem, and only needs to be converged with respect to the Brillouin zone discretization parameter N (and, in the case of defects with non-compact support, the domain truncation parameter). We demonstrated in the Appendix A that this method can be interpreted as a natural generalization of the complex-scaling method to non-parabolic dispersion relations.

Although we demonstrated only one- and two-dimensional tight-binding examples, the method fully applies to three-dimensional models described by continuous Hamiltonians (for instance, those arising in Density Functional Theory). Such an extension could be performed directly using an iterative method to compute the nonlinear eigenvalue problem (4), together with an iterative method to express the action of the unit cell resolvent $1/(z - H_{0,\mathbf{k}})$ appearing in the computation of R_0. This still requires a large number of computations if a dense sampling of the Brillouin zone is necessary. In this case, an alternative, more economical method would be to use Wannier functions to reduce to a tight-binding model, either exploiting periodicity [28], or using linear scaling approaches [29]. We hope to use these tools in future work to compute resonances in response functions of realistic solids (for instance, arising from time-dependent functional theory or GW methods).

Appendix A: connection with complex scaling

We reformulate our method to make the connection to complex scaling more explicit. Again for simplicity we consider a tight-binding model on a lattice Γ, with state space $\ell^2(\Gamma, \mathbb{C}^M)$, but our discussion generalizes immediately to continuous models. Each state $\psi = \{\psi_n\}_{n\in\Gamma}$ in this space can be equivalently seen as a function of the pseudo-momentum $\mathbf{k} \in \mathcal{B}$ through the Bloch (Fourier) transform, which we denote by $\{\psi(\mathbf{k})\}_{\mathbf{k}\in\mathcal{B}}$. We define a (non-unitary) transformation U in (a subset of) $\ell^2(\Gamma, \mathbb{C}^M)$ by the formula

$$(U\psi)(\mathbf{k}) = \psi(\mathbf{k} + i\mathbf{h}(\mathbf{k}))$$

for $\mathbf{k} \in \mathcal{B}$. Letting $\widetilde{H}_0 = UH_0U^{-1}$, we note that

$$(UH_0U^{-1}\psi)(\mathbf{k}) = (H_0U^{-1}\psi)(\mathbf{k} + i\mathbf{h}(\mathbf{k})) = H_{0,\mathbf{k}+i\mathbf{h}(\mathbf{k})}(U^{-1}\psi)(\mathbf{k} + i\mathbf{h}(\mathbf{k})) = H_{0,\mathbf{k}+i\mathbf{h}(\mathbf{k})}\psi(\mathbf{k}).$$

This allows us to compute analytic continuations of the Green function through the formula

$$\begin{aligned}
\langle\psi_1|\frac{1}{z-\hat{H}_0}|\psi_2\rangle &= \langle\hat{U}^{-*}\psi_1|\frac{1}{z-\hat{U}\hat{H}_0\hat{U}^{-1}}|\hat{U}\psi_2\rangle \\
&= \frac{1}{|\mathcal{B}|}\int_{\mathcal{B}} \overline{\psi_1}(\mathbf{k}+i\mathbf{h}(\mathbf{k}))\left(U^{-1}\frac{1}{z-UH_0U^{-1}}U\psi_2\right)(\mathbf{k}+i\mathbf{h}(\mathbf{k}))\det(1+\mathbf{h}'(\mathbf{k}))d\mathbf{k} \\
&= \frac{1}{|\mathcal{B}|}\int_{\mathcal{B}} \overline{\psi_1}(\mathbf{k}+i\mathbf{h}(\mathbf{k}))\frac{1}{z-H_{0,\mathbf{k}+i\mathbf{h}(\mathbf{k})}}\psi_2(\mathbf{k}+i\mathbf{h}(\mathbf{k}))\det(1+\mathbf{h}'(\mathbf{k}))d\mathbf{k}
\end{aligned}$$

from where the results of Section 4.2 follow.

We can now specialize this discussion to the case of the $d-$dimensional Hamiltonian $H_0 = -\frac{1}{2}\Delta$, which can be seen as a periodic operator with Brillouin zone $\mathcal{B} = \mathbb{R}^d$, and a single parabolic band $\varepsilon_{\mathbf{k}} = \frac{1}{2}|\mathbf{k}|^2$. In this case, the localization function χ is unnecessary; omitting it from (12) results in $\mathbf{h}(\mathbf{k}) = -\alpha\mathbf{k}$, defining the transformation $(U\psi)(\mathbf{k}) = \psi(\mathbf{k} - i\alpha\mathbf{k})$. It is instructive to compare this to the classical complex scaling transformation, defined in real space by $(U_\theta\psi)(e^{i\theta}x)$. Equivalently, this operator can be defined in Fourier space by $(U_\theta\psi)(\mathbf{k}) = e^{-i\theta}\psi(e^{-i\theta}\mathbf{k})$. Omitting the phase factor $e^{-i\theta}$ (which does not change the results) and expanding to first order in θ, this becomes $(U_\theta\psi)(\mathbf{k}) \approx \psi(\mathbf{k} - i\theta\mathbf{k})$, which is identical to the above with $\theta = \alpha$. The higher-order deviations are inconsequential, and come from the slightly different functional form of the complex deformation: complex scaling originates from a group action, whereas we do not find this requirement necessary in our deformation.

The above argument shows that the BCD method can be interpreted as natural generalization of the complex-scaling method to non-parabolic dispersion relations. Such a transformation in the reciprocal space is reminiscent of the generalized complex transformation, also named smooth exterior complex scaling, employed in molecular systems to solve some of the problems arising in the uniform complex scaling [30]. One important difference between our implementation of the method and complex scaling, however, is that we do not transform the whole operator $\hat{H} = \hat{H}_0 + \hat{V}$, but rather use the transformation only on $\hat{H}_0$ to compute its Green function, and deduce the Green function of $\hat{H}$ by a Dyson equation. This loses the "global" properties (we obtain resonances as a nonlinear eigenvalue problem, rather than a linear one in the case of complex scaling), but is much more flexible (since we do not need to transform $\hat{V}$, a possibly complicated operation). In simple cases however, it is possible to compute the transformation $\hat{U}$ and the non-Hermitian operator $\hat{\widetilde{H}} = \hat{U}\hat{H}\hat{U}^{-1}$ explicitly.

Appendix B: normalization of the resolvent

Consider an analytic family of matrices $A(z)$, and choose z_0 such that $A(z_0)$ has a simple eigenvalue 0. There are v, w such that $A(z_0)v = 0, A(z_0)^*w = 0$. We fix v and w to be normalized to 1. This means that

$A(z_0) = \begin{pmatrix} 0 & 0 \\ 0 & X \end{pmatrix}$ in the representation where the input space is split between v and $v^\perp$, and the output between w and $w^\perp$. X is invertible. Therefore,

$$A(z) \approx \begin{pmatrix} A_{11}(z-z_0) & A_{12}(z-z_0) \\ A_{21}(z-z_0) & X \end{pmatrix}$$

with $A_{11} = \langle w, A'(z_0)v\rangle$. The Schur complement is $A_{11}(z-z_0) + O((z-z_0)^2)$, with inverse $\frac{1}{z-z_0}A_{11}^{-1} + O(1)$, and it follows that

$$\begin{aligned} A(z)^{-1} &\approx \frac{1}{z-z_0}\begin{pmatrix} A_{11}^{-1} & 0 \\ 0 & 0 \end{pmatrix} + O(1) \\ &= \frac{1}{z-z_0}\frac{1}{\langle w, A'(z_0)v\rangle}|v\rangle\langle w| \end{aligned}$$

Applying to $A(z) = 1 - VR_0(z)$, we have $VR_0(z_0)\phi = \phi$ so we identify $v = \phi$. For w we solve $VR_0(z_0)^*\widetilde{\phi} = \widetilde{\phi}$ and so we identify w to $R_0(z_0)^*\widetilde{\phi}$, solution of $R_0(z_0)^*Vw = w$. The result is

$$R(z) = R_0(z)A(z)^{-1} \approx \frac{1}{z-z_0}\frac{1}{-\langle R_0(z_0)^*\widetilde{\phi}, VR_0'(z_0)\phi\rangle}|R_0(z_0)\phi\rangle\langle R_0(z_0)^*\widetilde{\phi}|$$

With $\psi(z_0) = R_0(z_0)\phi(z_0) = \overline{w}$, the residue of $(1 - VR_0(z))^{-1}$ at z_0 can readily be seen to be

$$(1 - VR_0(z))^{-1} \approx \frac{1}{-\langle\overline{\psi(z_0)}|VR_0'(z_0)|\varphi(z_0)\rangle}|\varphi(z_0)\rangle\langle\overline{\psi(z_0)}|\frac{1}{z-z_0}$$

which gives the following condition to have (4):

$$\langle\overline{\psi(z_0)}|\hat{V}\hat{R}_0'(z_0)|\varphi(z_0)\rangle = -1 \tag{14}$$

Note that $\phi \neq \widetilde{\phi}$. If H is real, then $R^*(z) = \overline{R}(z)$ and therefore $\widetilde{\phi} = \overline{\phi}$ and the residual is of the form $|\psi\rangle\langle\overline{\psi}|$.

Acknowledgments

This project has received funding from the European Research Council (ERC) under the European Union's Horizon 2020 research and innovation programme (grant agreement No 810367). Stimulating conversations with Mi-Song Dupuy and Sonia Fliss are gratefully acknowledged.

References

[1] Semyon Dyatlov and Maciej Zworski. *Mathematical theory of scattering resonances*, volume 200. American Mathematical Soc., 2019.

[2] G. Gamow. Zur quantentheorie des atomkernes. *Zeitschrift für Physik A Hadrons and Nuclei*, 51:204–212, 1928. 10.1007/BF01343196.

[3] Tore Berggren and Patric Lind. Resonant state expansion of the resolvent. *Phys. Rev. C*, 47(2):768–778, Feb 1993.

[4] Keita Sasada, Naomichi Hatano, and Gonzalo Ordonez. Resonant Spectrum Analysis of the Conductance of Open Quantum System and Three Types of Fano Parameter. *J.Phys.Soc.Jap.*, 80:104707, 2011.

[5] Takayuki Myo, Akira Ohnishi, and Kiyoshi Kato. Resonance and Continuum Components of the Strength Function. *Progress of Theoretical Physics*, 99(5):801–817, 1998.

[6] P. Lind, R. J. Liotta, E. Maglione, and T. Vertse. Resonant state expansions of the continuum. *Zeitschrift für Physik A Hadrons and Nuclei*, 347(4):231–236, 1994.

[7] Oleg I. Tolstikhin, Valentin N. Ostrovsky, and Hiroki Nakamura. Siegert Pseudo-States as a Universal Tool: Resonances, S Matrix, Green Function. *Phys. Rev. Lett.*, 79(11):2026–2029, Sep 1997.

[8] J.G. Muga, J.P. Palao, B. Navarro, and I.L. Egusquiza. Complex absorbing potentials. *Physics Reports*, 395(6):357–426, 2004.

[9] Alessandro Cerioni, Luigi Genovese, Ivan Duchemin, and Thierry Deutsch. Accurate complex scaling of three dimensional numerical potentials. *The Journal of Chemical Physics*, 138(20):204111, 2013.

[10] Dan Givoli. *Numerical methods for problems in infinite domains*. Elsevier, 2013.

[11] Anne-Sophie Bonnet-Ben Dhia, Sonia Fliss, and Yohanes Tjandrawidjaja. Numerical analysis of the Half-Space Matching method with Robin traces on a convex polygonal scatterer. In *Maxwell's equations*. De Gruyter, 2018.

[12] Christian Gérard. Resonance theory for periodic schrödinger operators. *Bulletin de la Société Mathématique de France*, 118(1):27–54, 1990.

[13] Vu Hoang. The limiting absorption principle for a periodic semi-infinite waveguide. *SIAM J. Appl. Math.*, 71:791–810, 2011.

[14] Patrick Joly, Jing-Rebecca Li, and Sonia Fliss. Exact boundary conditions for periodic waveguides containing a local perturbation. *Communications in Computational Physics*, 1(6):945–973, 2006.

[15] Ruming Zhang. Numerical methods for scattering problems in periodic waveguides. *Numerische Mathematik*, 148(4):959–996, 2021.

[16] J. M. Combes and L. Thomas. Asymptotic behaviour of eigenfunctions for multiparticle Schrödinger operators. *Communications in Mathematical Physics*, 34(4):251–270, December 1973.

[17] Michael Reed and Barry Simon. *Methods of modern mathematical physics. I: Functional Analysis*, volume 3. Elsevier, 1979.

[18] Stefan Güttel and Françoise Tisseur. The nonlinear eigenvalue problem. *Acta Numerica*, 26:1–94, 2017.

[19] Henri Alloul. *Introduction to the Physics of Electrons in Solids*. 01 2011.

[20] Hendrik J. Monkhorst and James D. Pack. Special points for brillouin-zone integrations. *Phys. Rev. B*, 13:5188–5192, Jun 1976.

[21] Mohsin Javed and Lloyd N. Trefethen. A trapezoidal rule error bound unifying the Euler–Maclaurin formula and geometric convergence for periodic functions. *Proceedings of the Royal Society A: Mathematical, Physical and Engineering Sciences*, 470(2161):20130571, January 2014.

[22] Eric Cancès, Virginie Ehrlacher, David Gontier, Antoine Levitt, and Damiano Lombardi. Numerical quadrature in the Brillouin zone for periodic Schrödinger operators. *Numerische Mathematik*, 144:479–526, January 2020.

[23] Naomichi Hatano, Keita Sasada, Hiroaki Nakamura, and Tomio Petrosky. Some Properties of the Resonant State in Quantum Mechanics and Its Computation. *Progress of Theoretical Physics*, 119(2):187–222, 02 2008.

[24] N. A. Pike and D. Stroud. Tight-binding model for adatoms on graphene: Analytical density of states, spectral function, and induced magnetic moment. *Physical Review B*, 89(11), Mar 2014.

[25] Mi-Song Dupuy and Antoine Levitt. Finite-size effects in response functions of molecular systems. *arXiv preprint arXiv:2102.09841*, 2021.

[26] Matthew Colbrook, Andrew Horning, and Alex Townsend. Computing spectral measures of self-adjoint operators. *SIAM Review*, 63(3):489–524, 2021.

[27] Susanne Irmer, Denis Kochan, Jeongsu Lee, and Jaroslav Fabian. Resonant scattering due to adatoms in graphene: Top, bridge, and hollow positions. *Phys. Rev. B*, 97:075417, Feb 2018.

[28] Nicola Marzari, Arash A Mostofi, Jonathan R Yates, Ivo Souza, and David Vanderbilt. Maximally localized wannier functions: Theory and applications. *Reviews of Modern Physics*, 84(4):1419, 2012.

[29] Laura E. Ratcliff, William Dawson, Giuseppe Fisicaro, Damien Caliste, Stephan Mohr, Augustin Degomme, Brice Videau, Viviana Cristiglio, Martina Stella, Marco D'Alessandro, Stefan Goedecker, Takahito Nakajima, Thierry Deutsch, and Luigi Genovese. Flexibilities of wavelets as a computational basis set for large-scale electronic structure calculations. *The Journal of Chemical Physics*, 152(19):194110, 2020.

[30] Luigi Genovese, Alessandro Cerioni, Maxime Morinière, and Thierry Deutsch. Identification of resonant states via the generalized virial theorem, 2015.